

Velocity shear, turbulent saturation, and steep plasma gradients in the scrape-off layer of inner-wall limited tokamaks

Federico D. Halpern* and Paolo Ricci
*École Polytechnique Fédérale de Lausanne (EPFL),
 Swiss Plasma Center, CH-1015 Lausanne, Switzerland*

The narrow power decay-length (λ_q), recently found in the scrape-off layer (SOL) of inner-wall limited (IWL) discharges in tokamaks, is studied using 3D, flux-driven, global two-fluid turbulence simulations. The formation of the steep plasma profiles measured is found to arise due to radially sheared $\mathbf{E} \times \mathbf{B}$ poloidal flows. A complex interaction between sheared flows and outflowing plasma currents regulates the turbulent saturation, determining the transport levels. We quantify the effects of sheared flows, obtaining theoretical estimates in agreement with our non-linear simulations. Analytical calculations suggest that the IWL λ_q is roughly equal to the turbulent correlation length.

Sheared flows can significantly affect the properties of turbulence in magnetically confined plasmas. These effects are observed in many plasma configurations, an archetype of such phenomena being the spontaneous formation of the high-confinement (H-)mode barrier at the edge of tokamak plasmas [1]. Turbulent suppression typically occurs when the radial shearing rate of the $\mathbf{E} \times \mathbf{B}$ plasma flows, $\omega_{\mathbf{E} \times \mathbf{B}} = dv_{\mathbf{E} \times \mathbf{B}}/dr$ ($v_{\mathbf{E} \times \mathbf{B}} = \mathbf{E} \times \mathbf{B}/B^2$), is of the order of the linear growth rate of the turbulent modes [2, 3]. Understanding the effects of sheared flows is paramount for attaining a fusion reactor, in particular due to their typically beneficial effects upon plasma energy confinement and stability.

The present letter deals with radially sheared $\mathbf{E} \times \mathbf{B}$ flows in the open magnetic field line region of tokamak devices, known as the scrape-off layer (SOL). In this region of the device, the balance between cross-field heat transport against parallel streaming along magnetic field lines gives rise to exponentially decaying power profiles with a characteristic length $\lambda_q = -(d_x \ln q_{||})^{-1}$ ($q_{||} \sim nc_s T$, with $c_s = \sqrt{(T_e + T_i)/m_i}$, is the power flowing along the magnetic field lines towards the device walls). As opposed to the confined plasma region, where we seek to use sheared flows to minimize turbulent transport, SOL turbulence can help avoid a too narrow power exhaust channel.

We concentrate on the inner-wall limited (IWL) geometry, where the plasma makes contact with the inner-wall of the device. This configuration will be used as a start-up plasma scenario in ITER before standard X-point configuration is attained [4]. It was originally assumed that the ITER IWL SOL could be described with a single-exponential λ_q of a few cm's [5]. Recent IWL experiments demonstrated that the SOL plasma profiles have a double-exponential decay length structure. In effect, in the near-SOL just outside the confined plasma region, λ_q is an order of magnitude smaller than expected [6–10]. We refer to this steep gradient region as the "narrow heat-flux feature". A multi-device study projects that the ITER IWL near-SOL λ_q will be about 4mm, and prompted a redesign of the inner-wall tiles to accommo-

date for the significantly smaller than expected λ_q [11].

Herein we demonstrate that the steep gradients in the narrow heat-flux feature can arise due to radially sheared $\mathbf{E} \times \mathbf{B}$ poloidal flows present at the interface between the confined plasma region and the SOL. We observe this phenomenon in 3D flux-driven turbulence simulations of plasma dynamics in the IWL configuration. Despite the strongly sheared flows, we find a relative fluctuation amplitude of about 20% within the narrow feature in the simulations, which is consistent with experimental observations. The most peculiar and surprising aspect of the simulated dynamics is the role of sheath currents and their interaction with the sheared turbulent flows in regulating cross-field turbulent transport. Considering these phenomena, we develop a reduced transport model capturing the physical mechanisms at play within the narrow feature. The resulting λ_q is intimately linked to the turbulent correlation length.

The formation of a narrow heat-flux feature is demonstrated using 3D flux-driven turbulence simulations of plasma dynamics in the IWL configuration. The non-linear simulations allow us to extract and understand the variation of the near-SOL λ_q with the plasma parameters. We make use of the drift-reduced Braginskii equations [12], which arise from applying the orderings $d/dt \ll \omega_{ci}$ ($\omega_{ci} = eB/m_i$ is the ion gyrofrequency) and $k_{\perp} \gg k_{||}$ to the Braginskii fluid equations [13]. We consider the simplest possible model that can be used to recover the narrow heat-flux feature, *i.e.* cold ions, a large aspect ratio torus with circular geometry, and we use the Boussinesq approximation. This entails the physics of drift and ballooning modes, which can be destabilized either by finite resistivity or inertia. The model equations for conservation of density n , vorticity $\Omega = \nabla_{\perp}^2 \phi$, parallel electron and ion velocities $v_{||e,i}$, and electron temperature T_e read

$$\frac{dn}{dt} = \frac{2}{eB} \left[\hat{C}(p_e) - en\hat{C}(\phi) \right] - \nabla \cdot (nv_{||e}\hat{\mathbf{b}}) + D_n \nabla_{\perp}^2 n + S_n \quad (1)$$

$$\frac{d\Omega}{dt} = \frac{2B}{nm_i} \hat{C}(p_e) + \frac{B^2}{nm_i} \nabla \cdot (j_{||}\hat{\mathbf{b}}) - v_{||i} \nabla_{||} \Omega$$

$$+ D_\Omega \nabla_\perp^2 \Omega + \frac{B}{3nm_i} \hat{C}(G_i) \quad (2)$$

$$\frac{dv_{\parallel e}}{dt} = \frac{ej_{\parallel}}{\sigma_{\parallel} m_e} + \frac{e \nabla_{\parallel} \phi}{m_e} - \frac{\nabla_{\parallel} p_e}{nm_e} - \frac{0.71 \nabla_{\parallel} T_e}{m_e} - v_{\parallel e} \nabla_{\parallel} v_{\parallel e} + D_{v_{\parallel e}} \nabla_\perp^2 v_{\parallel e} - \frac{2 \nabla_{\parallel} G_e}{3nm_e} \quad (3)$$

$$\frac{dv_{\parallel i}}{dt} = - \frac{\nabla_{\parallel} p_e}{n} - v_{\parallel i} \nabla_{\parallel} v_{\parallel i} + D_{v_{\parallel i}} \nabla_\perp^2 v_{\parallel i} - \frac{2 \nabla_{\parallel} G_i}{3nm_i} \quad (4)$$

$$\begin{aligned} \frac{dT_e}{dt} = & \frac{4}{3} \frac{T_e}{eB} \left[\frac{7}{2} \hat{C}(T_e) + \frac{T_e}{n} \hat{C}(n) - e \hat{C}(\phi) \right] \\ & + \frac{2T_e}{3en} \left[0.71 \nabla \cdot (j_{\parallel} \hat{\mathbf{b}}) - en \nabla \cdot (v_{\parallel e} \hat{\mathbf{b}}) \right] \\ & - v_{\parallel e} \nabla_{\parallel} T_e + \chi_{\perp, e} \nabla_\perp^2 T_e + \chi_{\parallel, e} \nabla_\parallel^2 T_e + S_{T_e} \end{aligned} \quad (5)$$

In these equations, $df/dt = \partial_t f / \partial t + \{ \phi, f \} / B$, we use the Poisson bracket $\{g, f\} = \hat{\mathbf{b}} \cdot (\nabla g \times \nabla f)$, and the curvature operator $\hat{C}(f) = (B/2)(\nabla \times (\hat{\mathbf{b}}/B))$. The unit magnetic field vector is $\hat{\mathbf{b}} = \mathbf{B}/B$, $j_{\parallel} = en(v_{\parallel i} - v_{\parallel e})$ is the parallel current, and σ_{\parallel} is the Spitzer conductivity. The coordinate system is given by the poloidal length, radial, and toroidal angle coordinates ($y = \theta a$, x , φ). S_{T_e} and S_n represent source terms used to inject density and temperature into the simulation domain. The numerical implementation of 1–5, including the definition of the gyroviscous terms $\sim G_{e,i}$ and other dissipative contributions, is described in detail in Ref. 14. (It has been checked that the artificial dissipation terms do not affect the simulation results.) Sheath boundary conditions, modeling the interface between the SOL plasma and the vessel walls, are applied at the entrance of the magnetized pre-sheath where the ion drift approximation breaks down [15].

Simulations are carried out within the parameter range $\rho_\star^{-1} = R/\rho_{s0} = 250\text{--}1000$, $\nu = e^2 n_{e,LCFS} c_s / (m_i \sigma_{\parallel} R) = 0.01, 0.1, 1$, $q = 4\text{--}16$, $m_e/m_i = 1/200$, with $a/R \approx 1/4$ ($q \approx (r/R)(B_\phi/B_\theta)$ is the magnetic safety factor, while $\rho_{s0} = c_{s0}/\omega_{ci}$, $c_{s0} = \sqrt{T_{e,LCFS}/m_i}$, and $\omega_{ci} = eB/m_i$). The simulation parameters $\rho_\star = 2000$, $\nu = 0.01$ roughly translate to the IWL SOL parameters of Alcator C-Mod ($R_0 = 0.67\text{m}$, $B_0 = 4\text{T}$, $T_{e,LCFS} = 25\text{eV}$, $n_{e,LCFS} = 10^{19}\text{m}^{-3}$). Using a simulation with $\rho_\star^{-1} = 500$, $q = 4$, and $\nu = 0.01$, e.g. corresponding to C-Mod parameters but with $B_0 = 1\text{T}$, we illustrate the basic physics mechanisms giving rise to the narrow heat-flux feature. The simulation domain entails an annular volume representing the plasma edge and the SOL, where an infinitely thin wedge acts as a limiter on the high-field-side. Temperature and density are added within the plasma edge using poloidally uniform, radially Gaussian sources (S_{T_e} and S_n) of radial width $5\rho_{s0}$ and placed at the inner boundary of the simulation domain. The plasma profiles steepen due to the action of the sources, driving turbulent modes that fill the SOL with plasma. Figure 1 shows steady-state, poloidally and toroidally averaged, radial profiles of $nc_s T_e$ showing a very clear break in slope about $20\rho_{s0}$ away from the LCFS ($nc_s T_e \sim q_{\parallel}$ near the

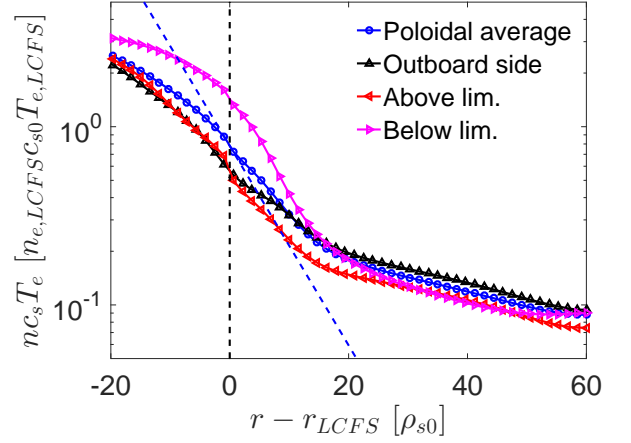


FIG. 1. Time averaged radial profiles of $nc_s T_e$, computed using (a) the entire poloidal cross-section (blue dotted line), (b) the equatorial outboard side of the device (black line with triangles), and (c) just above (red line with left-triangles) and (d) below the limiter (magenta line with right-triangles). Data obtained from the quasi steady-state phase of a simulation with $q = 4$, $\rho_\star^{-1} = 500$, $\nu = 0.01$.

limiter). The near SOL has $\lambda_q \approx 8\rho_{s0}$, which is equivalent to about 4mm in C-Mod ($B = 4\text{T}$, $T_{e,LCFS} \approx 25\text{eV}$) and agrees with experimental measurements [11]. From here onwards, we consider time, poloidally and toroidally averaged quantities (denoted with angled brackets $\langle \rangle$) in order to highlight the main physical mechanisms at play.

The radial component of the steady-state electric field, $\langle E_x \rangle = -\partial_x \langle \phi \rangle$ has opposite signs in the SOL and in the plasma edge. In the SOL, the interaction between the plasma and the sheath gives $\langle \phi \rangle \sim \Lambda \langle T_e \rangle / e$ ($\Lambda \approx 3$), i.e. $\partial_x \langle \phi \rangle > 0$, while in the plasma edge $\partial_x \langle \phi \rangle < 0$. As a result, $\langle \phi \rangle$ varies significantly around the LCFS, giving rise to a poloidal velocity shear layer in our simulations. In Fig. 2, the shearing rate $\omega_{\mathbf{E} \times \mathbf{B}} = \rho_\star^{-1} |\langle \phi \rangle''| c_s / R$ is compared against the reference ballooning growth rate $\gamma_b = \sqrt{2 \langle T_e \rangle / (\rho_\star L_p)} c_s / R$ ($L_p = -d_x \ln \langle p \rangle$). The shear layer effectively divides the edge of the plasma into 3 regions: (a) the plasma edge, where γ_b is comparable or larger than $\omega_{\mathbf{E} \times \mathbf{B}}$, (b) the near-SOL, where drift and ballooning type modes are strongly linearly stable due to the velocity shear layer, and (c) the far SOL, where $\omega_{\mathbf{E} \times \mathbf{B}}$ is weak. The latter region was extensively described in our previous studies [16, 17].

We typically find $\Lambda \langle T_e \rangle > \langle \phi \rangle$ at the LCFS of our simulations, which is consistent with Langmuir probe measurements in the near-SOL of TCV and COMPASS [8, 9]. This phenomenon, in fact, suggests that parallel currents flowing out of the plasma play an important in the near-SOL, since by charge conservation $j_\perp / L_\perp \sim j_\parallel / L_\parallel$. This simple heuristic argument immediately relates the near-SOL width, which should be similar to L_\perp , to the safety factor $q \sim 1/B_\theta$. Indeed, a simulation scan over $q = 4\text{--}$

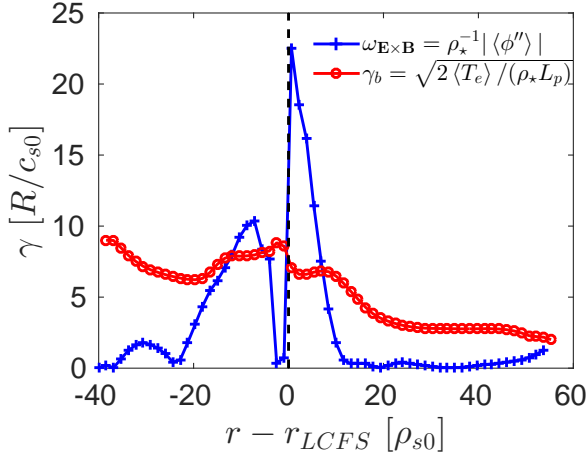


FIG. 2. Radial profiles of $\omega_{\mathbf{E} \times \mathbf{B}} = \rho_*^{-1} |\langle \phi \rangle''|$, and the ballooning growth rate, $\gamma_b = \sqrt{2 \langle T_e \rangle / (\rho_* L_p)}$. Computed from a simulation with $q = 4$, $\rho_*^{-1} = 500$, $\nu = 0.01$.

16, shown in Fig. 3, confirms that $\lambda_q / \rho_s \propto q$ at fixed $\nu = 0.01$ and $\rho_*^{-1} = 500$. The error bars give the root-mean-square deviation obtained from fitting $\langle n c_s T_e \rangle$ over a time interval of $40 R_0 / c_{s0}$.

Additional simulation scans have been carried out varying ν and ρ_* at fixed $q = 4$. In the first case, the resistivity only has an effect when $\nu \sim 1$, in which case we observe weaker j_{\parallel} near the limiter and an increased radial transport. Within the explored parameter range, we find little variation of λ_q / ρ_s with ρ_* , which suggests a weak dependence on the normalized plasma size.

To gain further insight on the role of the outflowing currents, we concentrate on the charge balance in the system, Eq. 2. This is illustrated in Fig. 4, where we have separated the contributions of all the terms in the vorticity equation (including numerical dissipative terms), as radial profiles. We observe that the parallel current contribution, $\langle B^2 \nabla \cdot j_{\parallel} / (n m_i) \rangle$, strongly affects the charge balance in the near-SOL. The parallel currents are mostly compensated through a polarization contribution $\sim \langle \{\phi, \Omega\} / B \rangle$, while other terms play a minor role. The curvature term $2 \langle B \hat{C}(p_e) / (n m_i) \rangle$ plays an important role in the far-SOL, consistent with blob filament motion [18]. On the other hand, the radial dissipative terms become noticeable near the LCFS due to the steep gradients of the radial $\langle \Omega \rangle$ profile – it has been tested that decreasing the radial diffusion steepens the profile by about $1 \rho_{s0}$, which is within the 95% confidence interval of the λ_q fit.

We now propose a reduced model predicting λ_q , based upon a balance between the j_{\parallel} and j_{\perp} contributions. Our objective is to obtain the transport levels within the narrow heat-flux feature. The perturbed electrostatic potential is determined through the vorticity balance, allowing us to evaluate the near-SOL $\mathbf{E} \times \mathbf{B}$ velocity. Consider a

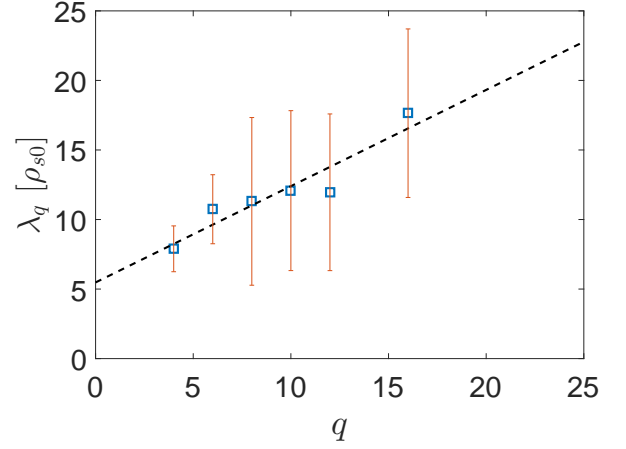


FIG. 3. Simulated narrow-feature widths in simulations with $q = 4$ –16, $\rho_*^{-1} = 500$, $\nu = 0.01$.

steady-state equation balancing parallel and polarization current terms at the LCFS. Integrating along the field line, and neglecting parallel mode anisotropy, we obtain

$$\frac{1}{B^2} \{\phi, \Omega\} = \frac{c_s \omega_{ci}}{L_{\parallel}} \exp\left(\frac{e \delta \phi_{fl}}{T_e}\right), \quad (6)$$

where we have used the Gauss' theorem and simplified the sheath current $j_{sh} = n c_s (1 - \exp(\Lambda - e \phi / T_e)) \approx n c_s \exp(e \delta \phi_{fl} / T_e)$ ($\delta \phi_{fl} = \Lambda T_e / e - \phi$). The simulation results indicate that the polarization current contribution is dominated by a radially sheared convection of vorticity. Taking a poloidal average, we recover the expression

$$\left\langle \frac{1}{B^2} \frac{\partial}{\partial x} \left(\tilde{\Omega} \frac{\partial \tilde{\phi}}{\partial y} \right) \right\rangle \approx \left\langle \frac{c_s \omega_{ci}}{L_{\parallel}} \exp\left(\frac{e \delta \phi_{fl}}{T_e}\right) \right\rangle, \quad (7)$$

with the tildes indicating perturbed quantities. This step points out that it is the radial shear of the turbulent motion that allows diverging parallel currents to arise. The currents flowing into the sheath, in turn, allow the potential to decouple from the temperature profile. The interaction with the closed magnetic field line region, where the electric field has the opposite sign than in the SOL, leads thereafter to the radially sheared electric field characteristic of the narrow heat-flux feature.

Next, we estimate $\tilde{\Omega} = -k_{\perp}^2 \tilde{\phi}$, and $\partial_x \sim k_x$ and $\partial_y \sim k_y$, which leads to the radial $\mathbf{E} \times \mathbf{B}$ velocity of turbulent structures propagating across the narrow feature

$$\langle \tilde{v}_{\mathbf{E} \times \mathbf{B}, x} \rangle^2 \approx \left\langle \frac{c_s \omega_{ci}}{L_{\parallel}} \frac{k_y}{k_x k_{\perp}^2} \exp\left(\frac{e \delta \phi_{fl}}{T_e}\right) \right\rangle. \quad (8)$$

The turbulent flux follows immediately from the estimate $\langle \Gamma_{\perp} \rangle \approx \langle \tilde{v}_{\mathbf{E} \times \mathbf{B}, x} \rangle$. The amplitude of the fluctuations traversing the narrow feature from the edge is estimated as $\langle \tilde{p} \rangle \sim \langle p \rangle / (k_x \lambda_q)$ [19, 20]. Then, the near-SOL width can be obtained by balancing $\nabla \cdot \langle \Gamma_{\perp} \rangle$ against the sheath

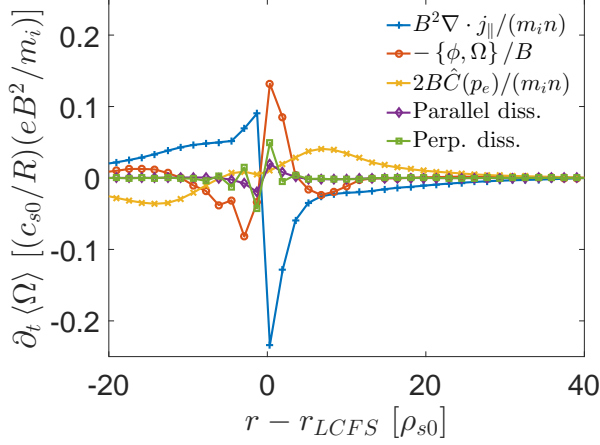


FIG. 4. Charge balance contributions from parallel currents (blue line with dots), vorticity convection (red line with crosses), curvature effects (yellow line with x's), parallel (purple line with diamonds) and perpendicular (green line with squares) dissipation terms. Computed from quasi steady-state phase of a simulation with $q = 4$, $\rho_{\star}^{-1} = 500$, $\nu = 0.01$.

contribution $\nabla_{\parallel} \cdot \langle \Gamma_{\parallel} \rangle \approx \langle p c_s \exp(e\delta\phi_{fl}/T_e) \rangle / L_{\parallel}$. The assumption of parallel convection rather than conduction is justified in the case of weak poloidal plasma gradients, which was an assumption of our analysis. The result is

$$\lambda_q = \left\langle \frac{k_y}{k_x^3 k_{\perp}^2} \frac{L_{\parallel}}{\rho_s} \exp\left(\frac{-e\delta\phi_{fl}}{T_e}\right) \right\rangle^{1/4} \approx \frac{k_x^{-1}}{2} \left(\frac{q}{\rho_{\star}}\right)^{1/4}. \quad (9)$$

In the last expression, we replaced $L_{\parallel} = qR$ and we assumed that eddies have comparable radial and poloidal wavenumbers, *i.e.* $k_x \sim k_y \sim k_{\perp}$ around the LCFS. The near SOL wavenumber is consistent with simulation results, and with gas-puff imaging of SOL turbulence [21]. As the modes traverse into the far SOL, k_x decreases while k_y remains about constant. We also approximate $\exp(-e\delta\phi_{fl}/T_e)^{1/4} \approx 1/2$, based on the LCFS values consistently found throughout our simulation scan. The weak dependence obtained with respect to the plasma parameters can explain, in part, why it is difficult to vary the narrow feature width in experiments – the plasma parameters appear only indirectly, and through the radial correlation length $L_{rad} = \pi/k_x$. Equation 9 is the principal result of the model, and the simpler expression involving k_x^{-1} is evaluated using the radial eddy correlation length and compared against non-linear simulation results in Fig 5.

In conclusion, we propose that a narrow layer of radially-sheared poloidal flows, occurring within the near-SOL, is responsible for the steep plasma gradients recently measured in the IWL tokamak experiments. Non-linear, flux-driven turbulent simulations demonstrate the spontaneous formation of $\mathbf{E} \times \mathbf{B}$ shearing rates significantly surpassing the expected linear growth rate of the turbulent modes. Simulation results sug-

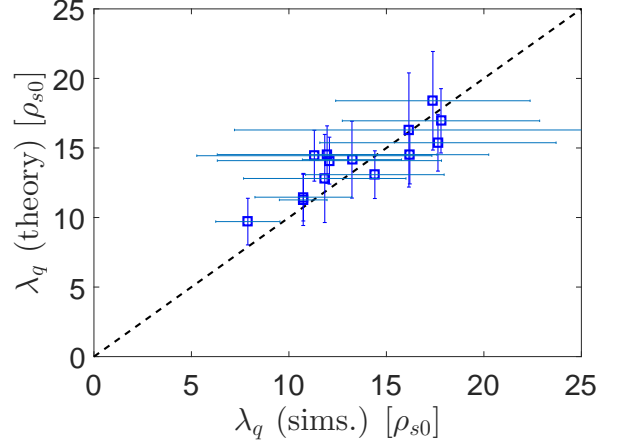


FIG. 5. Equation 9 is compared against non-linear simulation results.

gest that λ_q/ρ_s increases with $q \sim I_p^{-1}$, with weaker variation of λ_q with respect to ν or ρ_{\star} . The analysis of the simulations leads us to conclude that the turbulent saturation level can be determined by balancing the polarization currents driven by the turbulence against the parallel currents observed at the limiter. Analytical estimates lead to a gradient length of the order of the turbulent correlation length. The proposed transport model would suggest that a $\lambda_q \sim q \sim I_p^{-1}$ scaling (e.g. as in the Drift Heuristic Model [22]) can originate from the turbulent wavenumber. Inertial ballooning modes (IBM) are the most linearly unstable modes in the parameter regime $q = 4$, $\rho_{\star}^{-1} = 500$, $\nu \approx 0.01$ and with steep plasma gradients [23]. For instance, the wavenumber $k_{IBM}\rho_s \propto q^{-1}\gamma_b^{-1}$ together with Eq. 9 yield $\lambda_{q,IBM}/\rho_s \sim q^{5/6}\rho_{\star}^{-1/2}\nu^0$.

As a final remark, we highlight that our results lead to several testable predictions: (a) the turbulent intensity allows the outflow of parallel currents at the limiter, (b) the strength of the currents can be related to k_x , and (c) λ_q decreases with $q^{-1} \sim B_{\theta}$. Some of these features, such as the currents at the contact points, have been observed before in several devices. Dedicated experimental campaigns at C-Mod, DIII-D, and TCV will be used with the objective of validating the physical insights here presented.

Part of the simulations presented herein were carried out using the HELIOS supercomputer system at the Computational Simulation Centre of International Fusion Energy Research Centre (IFERC-CSC), Aomori, Japan, under the Broader Approach collaboration between Euratom and Japan, implemented by Fusion for Energy and JAEA. This work has been carried out within the framework of the EUROfusion Consortium and has received funding from the European Union's Horizon 2020 research and innovation program under grant agreement number 633053, and from the Swiss National Sci-

ence Foundation. The views and opinions expressed herein do not necessarily reflect those of the European Commission.

* federico.halpern@gmail.com

- [1] F. Wagner, G. Becker, K. Behringer, D. Campbell, A. Eberhagen, W. Engelhardt, G. Fussmann, O. Gehre, J. Gernhardt, G. v. Gierke, G. Haas, M. Huang, F. Karger, M. Keilhacker, O. Klüber, M. Kornherr, K. Lackner, G. Lisitano, G. G. Lister, H. M. Mayer, D. Meisel, E. R. Müller, H. Murmann, H. Niedermeyer, W. Poschenrieder, H. Rapp, H. Röhr, F. Schneider, G. Siller, E. Speth, A. Stäbler, K. H. Steuer, G. Venus, O. Vollmer, and Z. Yü, Phys. Rev. Lett. **49**, 1408 (1982).
- [2] H. Biglari, P. H. Diamond, and P. W. Terry, Physics of Fluids B **2**, 1 (1990).
- [3] K. H. Burrell, Physics of Plasmas **4**, 1499 (1997).
- [4] R. Pitts, S. Carpentier, F. Escourbiac, T. Hirai, V. Komarov, A. Kukushkin, S. Lisgo, A. Loarte, M. Merola, R. Mitteau, A. Raffray, M. Shimada, and P. Stangeby, Journal of Nuclear Materials **415**, S957 (2011), proceedings of the 19th International Conference on Plasma-Surface Interactions in Controlled Fusion.
- [5] A. Loarte, B. Lipschultz, A. Kukushkin, G. Matthews, P. Stangeby, N. Asakura, G. Counsell, G. Federici, A. Kallenbach, K. Krieger, A. Mahdavi, V. Philipps, D. Reiter, J. Roth, J. Strachan, D. Whyte, R. Döerner, T. Eich, W. Fundamenski, A. Herrmann, M. Fenstermacher, P. Ghendrih, M. Groth, A. Kirschner, S. Konoshima, B. LaBombard, P. Lang, A. Leonard, P. Monier-Garbet, R. Neu, H. Pacher, B. Pegourie, R. Pitts, S. Takamura, J. Terry, E. Tsitrone, the ITPA Scrape-off Layer, and D. P. T. Group, Nuclear Fusion **47**, S203 (2007).
- [6] G. Arnoux, T. Farley, C. Silva, S. Devaux, M. Firdaouss, D. Frigione, R. Goldston, J. Gunn, J. Horacek, S. Jachmich, P. Lomas, S. Marsen, G. Matthews, R. Pitts, M. Stamp, P. Stangeby, and J. Contributors, Nuclear Fusion **53**, 073016 (2013).
- [7] J. Horacek, P. Vondracek, R. Panek, R. Dejarnac, M. Komm, R. Pitts, M. Kocan, R. Goldston, P. Stangeby, E. Gauthier, P. Hacek, J. Havlicek, M. Hron, M. Imrisek, F. Janky, and J. Seidl, Journal of Nuclear Materials , 385 (2014).
- [8] F. Nespoli, B. Labit, I. Furno, G. Canal, and A. Fasoli, Journal of Nuclear Materials , 393 (2014).
- [9] R. Dejarnac, P. Stangeby, R. Goldston, E. Gauthier, J. Horacek, M. Hron, M. Kocan, M. Komm, R. Panek, R. Pitts, and P. Vondracek, Journal of Nuclear Materials **463**, 381 (2015), proceedings of the 21st International Conference on Plasma-Surface Interactions in Controlled Fusion Devices Kanazawa, Japan May 26-30, 2014.
- [10] P. Stangeby, C. Tsui, C. Lasnier, J. Boedo, J. Elder, M. Kocan, A. Leonard, A. McLean, R. Pitts, and D. Rudakov, Journal of Nuclear Materials **463**, 389 (2015), proceedings of the 21st International Conference on Plasma-Surface Interactions in Controlled Fusion Devices Kanazawa, Japan May 26-30, 2014.
- [11] M. Kocan, R. Pitts, G. Arnoux, I. Balboa, P. de Vries, R. Dejarnac, I. Furno, R. Goldston, Y. Gribov, J. Horacek, M. Komm, B. Labit, B. LaBombard, C. Lasnier, R. Mitteau, F. Nespoli, D. Pace, R. Panek, P. Stangeby, J. Terry, C. Tsui, and P. Vondracek, Nuclear Fusion **55**, 033019 (2015).
- [12] A. Zeiler, J. F. Drake, and B. Rogers, Physics of Plasmas **4**, 2134 (1997).
- [13] S. I. Braginskii, *Transport processes in a plasma*, edited by M. A. Leontovich, Reviews of Plasma Physics, Vol. 1 (Consultants Bureau, New York, 1965) p. 205.
- [14] F. Halpern, P. Ricci, S. Jolliet, J. Loizu, J. Morales, A. Masetto, F. Musil, F. Riva, T. Tran, and C. Wersal, Journal of Computational Physics **315**, 388 (2016).
- [15] J. Loizu, P. Ricci, F. D. Halpern, and S. Jolliet, Physics of Plasmas **19**, 122307 (2012).
- [16] F. D. Halpern, S. Jolliet, J. Loizu, A. Masetto, and P. Ricci, Physics of Plasmas **20**, 052306 (2013).
- [17] F. Halpern, P. Ricci, S. Jolliet, J. Loizu, and A. Masetto, Nuclear Fusion **54**, 043003 (2014).
- [18] S. I. Krasheninnikov, D. A. D'Ippolito, and J. R. Myra, Journal of Plasma Physics **74**, 679 (2008).
- [19] W. Horton, Rev. Mod. Phys. **71**, 735 (1999).
- [20] P. Ricci and B. N. Rogers, Physics of Plasmas **20**, 010702 (2013).
- [21] S. J. Zweben, J. A. Boedo, O. Grulke, C. Hidalgo, B. LaBombard, R. J. Maqueda, P. Scarin, and J. L. Terry, Plasma Physics and Controlled Fusion **49**, S1 (2007).
- [22] R. Goldston, Nuclear Fusion **52**, 013009 (2012).
- [23] A. Masetto, F. D. Halpern, S. Jolliet, and P. Ricci, Physics of Plasmas **19**, 112103 (2012).